ISSN 0001-4338, Izvestiya, Atmospheric and Oceanic Physics, 2015, Vol. 51, No. 6, pp. 585–598. © Pleiades Publishing, Ltd., 2015.
Original Russian Text © K.B. Moiseenko, N.A. Malik, 2015, published in Izvestiya AN. Fizika Atmosfery i Okeana, 2015, Vol. 51, No. 6, pp. 658–672.

Reconstruction of the Ashfall at Bezymyanny Volcano during the Eruption of December 24, 2006 by Using a Mesoscale Model of the Atmospheric Transport of Ash Particles

K. B. Moiseenko[a] and N. A. Malik[b]

[a] *Obukhov Institute of Atmosphere Physics, Russian Academy of Sciences, Pyzhevskii per. 3, Moscow, 119017 Russia*

e-mail: konst.dvina@mail.ru

[b] *Institute of Volcanology and Seismology, Far East Branch of the Russian Academy of Sciences, bul'v. Piipa 9, Petrpavlovsk-Kamchatsky, 683006 Russia*

Reveived September 4, 2014; in final form December 15, 2014

Abstract—Intensive volcanic eruptions of an explosive type are accompanied by release of a great amount of ash particles into the atmosphere. These particles are finely dispersed (<2 mm in size) products of magmatic melt fermentation, and their precipitation on the underlying surface is largely controlled by atmospheric transport. The present work proposes an approach to estimate the total released mass (TRM) of ash at minimal a priori data on dynamics of explosive process, on the basis of, first, direct numerical modeling of atmospheric transport and gravity precipitation of ash particles and, second, field observation data. To exemplify, the case study of the strong explosive eruption of Bezymyanny volcano on December 24, 2006 is considered (TRM > 3.8 Mt, height of eruptive column is 13–15 km above sea level). The results of the model calculations for this event are compared to independent TRM estimates by using standard methods based on the counting of precipitation areas.

Keywords: volcanic ash, Bezymyanny volcano, atmospheric transport, numerical simulation

DOI: 10.1134/S0001433815050072

INTRODUCTION

In estimating the geologic, atmospheric, and climatic effects of explosive eruptions [1–3], the knowledge of the total mass and composition of volcanic ash are important. Volcanic ash is represented by particles <2 mm in size, which are formed in magmatic melt dispersion and fragmentation of volcanic rocks during an eruption [4–6]. Ashfalls of a great volume are characteristic for volcanic eruptions of intermediate and felsic rocks, and many active volcanoes of the Kuril–Kamchatka region (Bezymyanny, Kizimen, Shiveluch, and others) are categorized in this group [5, 7]. The aim of the present work is to analyze the possible application of modern numerical models of atmospheric dynamics and transport to define the mass parameters of ash emission (total mass of emission, grain-size of ash, and ash distribution over altitude) and to reconstruct ash precipitation fields in the vicinities of active Kamchatkan volcanoes. The high-latitude positions of these volcanoes, the peculiarities of meteorological regime, and the complex relief cause a high variability of the atmospheric transport conditions and ash plume traces on the surface: these factors should be taken into account when computing the total released mass (TRM) for particular explosive events and eruptions in general.

A standard approach to defining ashfall mass implies the application of the well developed isopach method [8, 9]: the areas characterized by equal ash thickness (or mass per area unit) and confined by respective isolines are counted. In practice, however, the necessary number of sampling points and their optimal arrangement can hardly be achieved because of the volcano's remoteness, the considerable area of ashfall, and often the absence of necessary a priori information about the spatial characteristics of precipitated ash.

An alternative method of TRM estimation using sampling data is based on the numerical solution of the inverse problem of atmospheric transport at a set realistic wind and atmospheric turbulence fields in the vicinity of the volcano [10–13]. Practice shows that the application of atmospheric transport models for TRM estimation considerably reduces vagueness related to the considerable effect of the atmospheric factor on the spatial distribution and structure of ash-

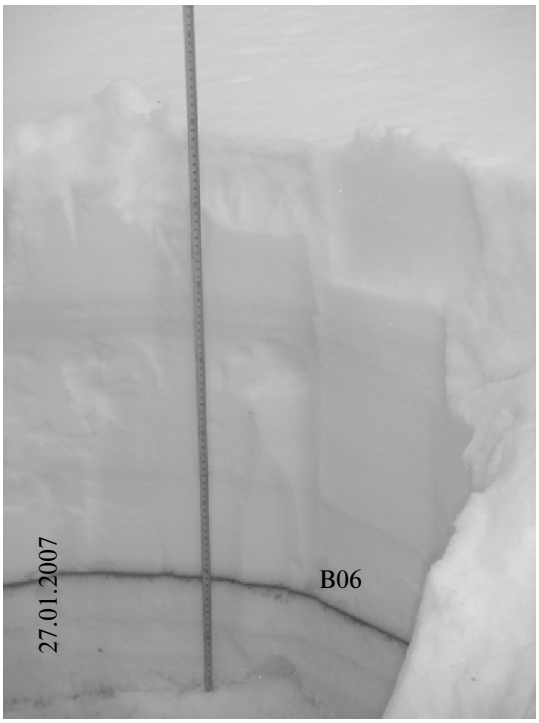

Fig. 1. Snow pit with ash bed (B06) after the eruption of Bezymyanny volcano on December 23–24, 2006 (image by N.A. Malik).

fall when field observations involve a relatively small part of the ashfall zone. However, such models as ASH-FALL [10, 11], HAZMAP [12], and TEPHRA2 [13], which are used for the solution of this problem, are oversimplified and inapplicable to areas of complex relief and/or the conditions of high spatial variability of wind and turbulence fields. In this respect, eruptions with relatively small explosive coefficients are used for studies when solid eruption products precipitate in the near zone, <30 km (the Vesuvius eruption of 472 BC [14]; the Cero Negro eruption of 1992 [15]; and the Plinian phase of the Pululagua eruption 2450 BC [16]).

Another problem in the application of the alternative approach is the high vagueness in computing the gravity precipitation rate of particles: this rate highly depends on particle shape and density, as well as on the parameters of ash aggregates forming from the finest disperse fractions. The simplest ashfall regression models [13, 14] are based on the assumption that the nonspherical parameter is constant [14] in the considered particle populations; however, this may lead to considerable and hardly controllable errors when reconstructing ashfall distribution and ash source parameters [15–19].

In the present work, we propose a numerical algorithm for the reconstruction of ashfall parameters in terms of a quite general problem statement, taking into account (a) the variations in aerodynamic parameters of particles within particular size classes and (b) the inhomogeneous distribution of released ash mass on altitude in the source (eruptive column). For computing atmospheric transport, we used the RAMS/HYPACT numerical hydrodynamic model complex [20–22]; it allows us to take into account the effects of orography and atmospheric conditions in general on ash precipitation in the mountain areas. The case study considered is the strong explosive eruption of Bezymyanny volcano on December 24, 2006 [17] (section 2). The solution of the inverse problem for this case study implies the reconstruction of particle mass spectrum in terms of a multiple regression model [18], with aerodynamic parameters of particles taken into consideration (section 3). The correct account of both controlling factors (distributions of ash mass on altitude and precipitation rates) allows us to considerably reduce the resulting errors when calculating ashfall parameters and the distribution of ash mass within the ashfall zone (section 4).

2. EXPLOSIVE EVENT AT BEZYMYANNY VOLCANO ON DECEMBER 24, 2006

The Bezymyanny volcano (55°58′ N, 160°36′ E, ~2600 m high: here and elsewhere, elevation is above sea level) is located in the central part of the Klyuchevskoy volcano group. Since its first historical eruption in October 1995, it is considered to be among the most active volcanoes in Kamchatka. Resulting from a paroxysmal eruption on March 30, 1956 [23], a large explosive crater formed; since then and up to the present, an extrusive dome has been growing there, with associated eruptions also occurring. Annually, one or two short-term explosive eruptions on average occur at the volcano; they are accompanied by the arising of eruptive columns by 6–15 km and the formation of pyroclastic flows of lengths up to 12.5 km [24, 25]. In 2006, two explosive eruptions of nearly the same intensity occurred: namely on May 9 and December 24.

2.1. Eruption of December 24, 2006

According to the Kamchatka Division of the Geophysical Survey, Russian Academy of Sciences (KD GS RAS), seismic preparation for this eruption began in late November 2006. Starting from December 23, 2006, 03:50 UTC, the first heated avalanches, accompanied by NE-directed ash plumes to altitudes of up to 4 km, were reported; since 23:50 UTC, large avalanches and explosions with ash rising up to 6.5 km were observed (Fig. 1). Based on seismic data, the culminating phase of the explosion took place on December 24 in the time interval of 09:20–10:10 UTC

Fig. 2. Ash cloud above Bezymyanny volcano during the initial phase of the eruption on December 23–24, 2006; view from Kozyrevsk settlement, 40 km NW of the volcano (a screenshot from video made by Kamchatkan Division of the Geophysical Survey, Russian Academy of Sciences).

(December 24, 21:17–22:10 LT). Due to nightfall, visual observation was impossible; however, the researchers at the Kozyrevsk seismic station observed lightning flashes and the mushroom-like eruptive column being risen by about 13–15 km high. According to satellite data, the ash cloud moved at an altitude of 9–10 km: it initially moved NE (azimuth ~40°), gradually changing to an ENE–E direction, and was observed at a distance of up to 850 km from the volcano [17].

In addition to ash precipitation from the eruptive cloud, a geologic effect of this eruption was pyroclastic flows (PFs) of lengths of 6.5 km and ~2.04 km^2 in an area in the SE sector of ash precipitations. PFs presumably came down immediately after the culmination of the explosion as a result of the gravity collapse of the eruptive column and the ejection of a short (625 × 200 m) lava flow on the SE slope of the volcanic edifice [25].

During the field season in January–March 2007, 40 areal samples (hereinafter, $i = 1, ..., 40$) of ash were collected (Fig. 2) at the distances of 23–105 km from the volcano, along and across the ashfall course; for these samples, ash mass was measured in terms of mass per area unit. Also, nine samples ($i = 41, ..., 49$) were collected in the zone where no ashfall was recorded: these sampling points were used to specify the boundary of ashfall zone, including those in numerical simulation. Based on ash sampling, we constructed an ashfall distribution map (Fig. 3); total ashfall area was ~8000 km^2. The sampling data also allowed us to reconstruct the variations in precipitated mass along two cross sections of the ash plume at the distances of about 40 and 95 km from the volcano (Fig. 4). For samples $i = 1,...16$, the total masses of particles from grain size fractions were measured; the grain size fractions (μm), namely F_2 (250–500), F_3 (125–250), F_4 (63–125), and $F_{<63}$, were revealed by screen analysis (Table 1).

2.2. Total Precipitated Mass

The total mass of precipitated ash was calculated by a piecewise-linear approximation of the empirical dependence $\log M_i - A_i^{1/2}$ (M_i is the mass of precipitated material within the i-th contour confining the area A_i) in accord with the technique of [9]. The obtained value of total precipitated ash was ~3.8×10^9 kg [18]. The given estimate is probably the lower limit of the total precipitated ash, because the finest fractions were not taken into account due to their removal beyond the ashfall zone identified from satellite images and sampling data (contour S in Fig. 3) in the form of eruptive clouds and plumes at substratospheric altitudes.

2.3. Atmospheric Conditions

Meteorological conditions in the area of the volcano during the eruption were controlled by a cyclone (Fig. 5) that slowly moved SE from the Sea of Okhotsk

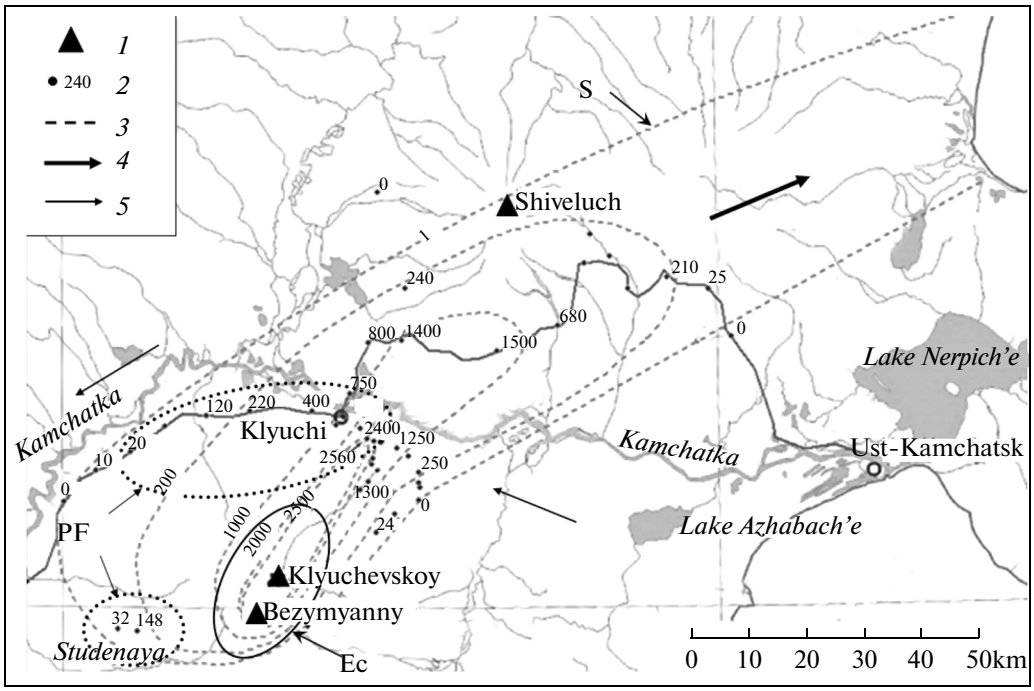

Fig. 3. Volcanic ash precipitation filed for the explosive event at Bezymyanny volcano on December 23–24, 2006, 09:20–10:10 UTC [17]. (*1*) Active volcanoes; (*2*) sampling points and precipitated ash masses, g/m^2; (*3*) isolines of mass, g/m^2; (*4*), (*5*) wind direction at the altitudes of near tropopause and <1.5 km, respectively. Ec is the schematic position of the eruptive cloud formed in the upper part of eruptive column 70 min after the eruption start (based on TERRA MODIS data, image made at 10:10 UTC in the thermal channel 20b); PF, zone of ash precipitated from the altitudes of >6 km (model calculations); S, boundary of the ash precipitation zone, based on NOAA satellite data.

and determined cloudy weather with snowfall in most of the Kamchatka Peninsula. Warm air advection at an altitude of <700 hPa manifested in the wind hodograph (Fig. 6a) in the form of a wind turn (which is characteristic for the warm sector) with an altitude in the SE–S–NW direction. In general, the baric field above Kamchatka Peninsula during the eruption can be characterized as small-gradient and relatively stable. Advection rates were therefore small in the entire altitude range (Fig. 6a), and the main part of ash particles precipitated at distances of up to 100 km in the form of a united NE-directed plume. A small amount of ash material precipitated in the W and NW directions due to the influence of low-altitude air flows rounding the mountain massif of Klyuchevskoy volcanic group on north, along the Kamchatka River valley (Fig. 3), and this determined the noticeable asymmetry of the precipitation plume (Fig. 4).

3. MODELS AND METHODS

3.1. RAMS Model

The RAMS numerical hydrodynamic model (Regional Atmospheric Modeling System, www.atmet.com) [23, 24] is used for weather forecast within a limited area and for studying atmospheric processes on a wide range of scales (from the hemispherical to turbulent vortices and convection in the boundary layer). However, in general, this model is applicable to mesometeorological processes (2–2000 km in altitude) and can be used to calculate meteorological fields in problems of the regional transport of pollutants. The spatial resolution of initial data on the topography and types of underlying surface is 30 × 30" and allows us to simulate airflow dynamics in the vicinity of a volcano with maximal detail.

3.2. HYPACT Model

The HYPACT model (HYbrid Particle Concentration Transport Model) [23, 25] is used to calculate the transport of passive pollutants by using the stochastic model of atmospheric turbulence [26, 27]. Turbulent variations in wind speed are calculated on the basis of model fields of wind, kinetic turbulence energy, and thermodynamic parameters. Transport is calculated by numerical integration over the time of the kinematic equations for a large amount (~10^5–10^7) of model particles representing elementary air volumes, with each of these volumes carrying certain mass of a tracer with similar aerodynamic parameters (in this

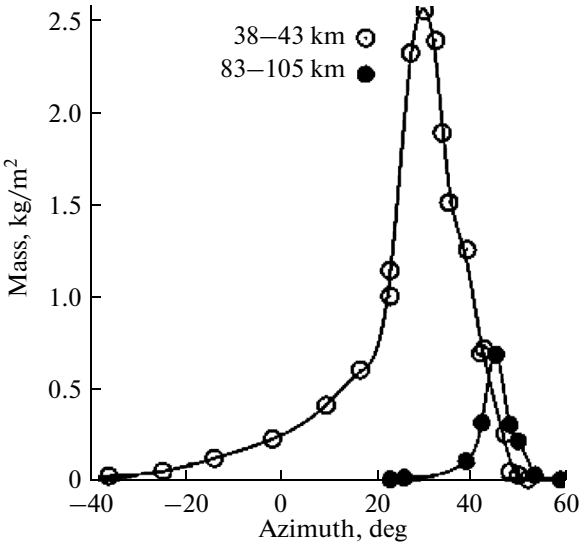

Fig. 4. Variations in mass of precipitated volcanic ash across ashfall zone's axis, based on the areal sampling at the distances of 38–43 and 83–105 km from the volcano. On the abscissa, the azimuth from volcano is indicated.

case, ash particles having the same density, shape, and mean size). If a particle reaches the Earth's surface, it is considered to be settled and then excluded from consideration. With the spatial positions of the model particles known at any concrete moment of time, we can calculate the mean volumetric concentration of suspended ash particles (or precipitated mass of particles) on the underlying surface at any spatial point. The model was applied to the computations of volcanic ash transport in [28] to simulate the eruption of Ruapehu volcano in New Zealand in 1995–1996.

3.3. Gravity Precipitation of Particles

The standard HYPACT code was supplemented with the block of gravity precipitation rate v_t of as particles in accord with the Wilson–Hang model [29]:

$$v_t(m) = \sqrt{2mg/(AC_d\rho_a)}, \quad (1)$$

where $m = \rho\pi d^3/6$ is the mass of a particle; $A = \pi d^2/4$ is the cross section area of a particle; d is the mean diameter of a particle; ρ is the mean density of a particle; g is free-fall acceleration; ρ_a is the density of surrounding air; and C_d is the coefficient of aerodynamic resistance:

$$C_d = \frac{24}{\mathrm{Re}} F^{-\alpha} + 2\sqrt{1.07 - F}, \quad (2)$$

where $\mathrm{Re} = \rho_a v_t d/\mu$ is the Reynolds number based on particle diameter (μ is the coefficient of air dynamic viscosity); $\alpha = 0.828$; $F = (D_m + D_s)/2D_l$ is the spheric-

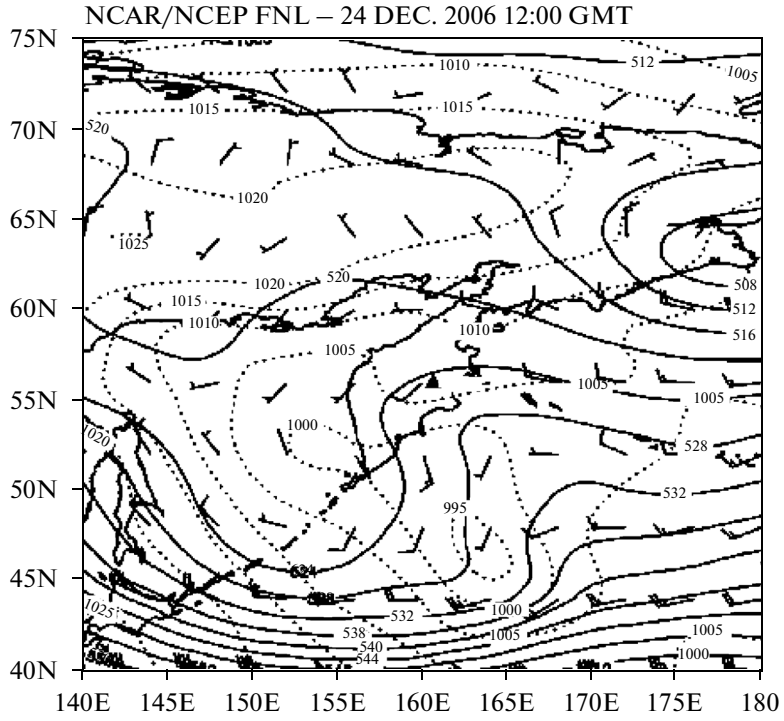

Fig. 5. Meteorological fields of NCEP FNL analysis as of December 24, 2006, 12:00 UTC: the field of 500 hPa geopotential (solid line); pressure at sea level (dashed line); wind at the altitude of 500 hPa (long tick mark means 10 m/s, short one means 5 m/s) (database at http://rda.icar.edu/datasets/ds083.2/).

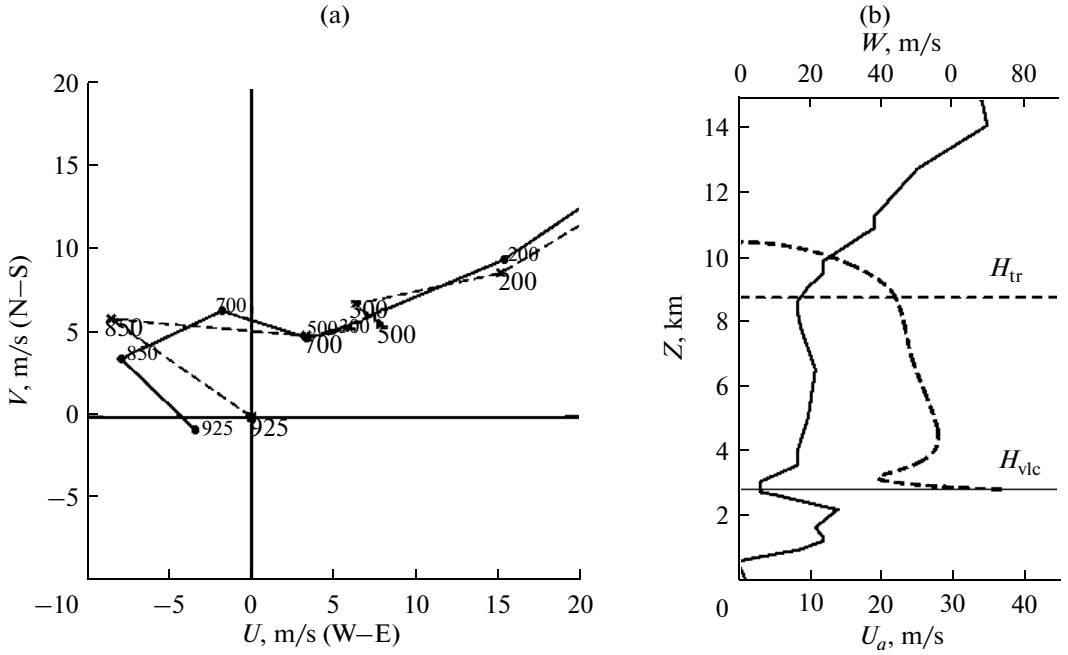

Fig. 6. Wind hodograph, based on the data from radioprobe in Klyuchi sett. (OBS) and the calculations on RAMS model, on the G3 grid (see Fig. 9 and section 3.6) as of December 24, 2006, 12:00 UTC (the nearest period to the culmination phase of eruption). *U* and *V* are the wind components in W–E and N–S directions, respectively. Notations on graphs denote altitudes above sea level, in mbar.

ity parameter; D_l, D_m, and D_s are the particle sizes along the main axes; $d = (D_m + D_s + D_l)/3$.

Studies show that for particles of sizes less than 500–1000 μm (finely dispersed ash fractions) atmospheric transport is made in an inertia-free mode, where particles are almost instantly involved into turbulent vortices [30, 31]. The influence of the precipitation rate is manifest in the general decrease in particle life within a particular vortex and hence can be seen in some decrease in the general dispersion of precipitating ash cloud [32, 33]. Taking into consideration that ash precipitation takes place from high altitudes under conditions of nearly quasi-laminar flow, the effect of wind shift in the evolution of the initially released cloud absolutely dominates at almost all altitudes, excluding the lower troposphere. The role of turbulence is reduced to smoothing the spatial gradients of the precipitated mass on "submesh" scales corresponding to the horizontal dimensions of atmospheric vortices in the inertial subzone of flow.

In general, within the desired range of $\rho = 2.2$–2.7 g/cm^3, which is characteristic for fine fractions of Bezymyanny volcano ashes, the main role in the v_t calculation is played by the parameter of nonsphericity (Fig. 7). Despite the assumption that the shape of particles was spherical ($F \approx 0.8$–0.9) in earlier works, including those that studied the Bezymyanny volcano [7], it is this parameter that, being correctly estimated, is critical for a successful reconstruction of precipitation rate spectrum, as was shown in [18]. The technique for the approximate estimation of the influence of particle shape on the precipitation rate in the absence of reliable numerical data on aerodynamic properties of particles will be considered in section 3.5.

3.4. Ash Ejection Source

Visual observations, including those for other eruptions of similar intensity at Bezymyanny volcano, suggest an insignificant influence of wind flow on the eruptive column dynamics for the explosive event under consideration. This suggestion is also supported by calculations from [18], using the PlumeRise integrated model of eruptive flow [34]: according to the results of these calculations, the rates of convective uplift of the gas suspension in nearly the entire altitude range within the eruptive column exceeded wind speed in the atmosphere (Fig. 6b). Following the methodology from [18], we used a two-layer model of a spatially uniform axisymmetric source ϖ with a temporally constant mass discharge; the source dimensions are found by the empirical dependence

$$\varpi: \quad R(z) = \begin{cases} R_c + \kappa(z - z_c), & z_c < z \le z_1 \\ R_2, & z_1 < z \le z_t \end{cases}, \qquad (3)$$

where R is the radius of the eruptive column; $\kappa = (R_2 - R_c)/(z_1 - z_c)$ is the coefficient of the eruptive flow expansion; $R_c = 150$ km is the radius of the crater; $z_c = 2.0$ km is the lower boundary of the source in accord with the smoothed (model) relief; $R_2 = 15$ km

is the mean radius of the eruptive cloud (contour Ec in Fig. 3) formed in the upper part of the column at the culmination phase of eruption (12–20 km; for this and the two subsequent parameters, the values in parentheses indicate the respective possible variation range); $z_1 = 8$ km is the mean size of the lower base of this eruptive cloud (6–9 km); and $z_t = 14$ km is the mean maximal altitude of this eruptive cloud (13–15 km). As was shown by numerical experiments, variations in R_1, R_2, and z_1, within the mentioned limits, lead to resultant estimates of ash release parameters within the value of one standard deviation for calculating with optimal geometric parameters of the source.

When conducting the model calculations, we used the step approximation (3) on z by the discrete set of spatially uniform sources ϖ_j:

$$\varpi_j: \ z \in Z_{\varpi_j} = [z_j, z_j + \Delta z], \ \bigcup_{j=1}^{N} \varpi_j = \Omega, \qquad (4)$$

where $\Delta z = 1$ km, $z_1 = z_c$, and $N = 12$, with the value of the mass discharge assumed to be equally distributed over the volume and time of source activity.

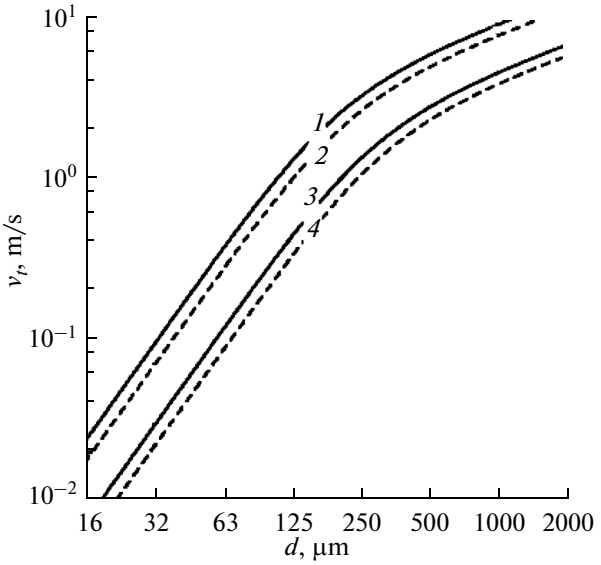

Fig. 7. Dependence of gravity precipitation rate (1) and (2) on particle grain size for different values of nonsphericity and particle density: (*1*) $F = 1$, $\rho = 2.7$ g/cm^3; (*2*) $F = 1$, $\rho = 2.0$ g/cm^3; (*3*) $F = 0.1$, $\rho = 2.7$ g/cm^3; (*4*) $F = 0.1$, $\rho = 2.0$ g/cm^3.

3.5. Regression Model

Samples collected after the eruption of December 24, 2006 contained particles of a size less than $d_{\max} = 500$ μm in an amount sufficient for grain size analysis. Hence, the following ash release parameters will be estimated: total released mass, $(\mathrm{TRM})_{<500}$; its distribution on altitude intervals, $(\mathrm{TRM})_{<500,j}$ ($j = 1,...N$), in terms of the model (3)–(4), and on fractions F_k distinguished by screen analysis, $(\mathrm{TRM})_k$, $k = k_1...k_2$ ($k_1 = 2$, $k_2 = 5$) for particles of $<d_{\max}$ in size (hereinafter, for the fraction $F_{<63}$, lowercase index 5 will be used). Bearing in mind the complex dynamics of explosive processes in general, the parameters sought will characterize the total effect of ash material discharge in the eruptive clouds and plumes for the entire considered period of December 23–24, 2006, with the dominant contribution from the culmination phase (eruptive cloud and PF ash clouds).

Let $\mathbf{y}_{\mathrm{obs}} = (y_{\mathrm{obs}}(\mathbf{r}_1)\ldots y_{\mathrm{obs}}(\mathbf{r}_M))$ and $\mathbf{y}^{(k)}_{\mathrm{obs}} = (y^{(k)}_{\mathrm{obs}}(\mathbf{r}_1)\ldots y^{(k)}_{\mathrm{obs}}(\mathbf{r}_{Mg}))$ denote the vectors of the measured bulk and total masses of particles, respectively, in particular the grain size fractions at sampling points $\mathbf{r}_i$. In the general case we have

$$y_{\mathrm{obs}}(\mathbf{r}_i) = \sum_{k=k_1}^{k_2} y^{(k)}_{\mathrm{obs}}(\mathbf{r}_i), \ i = 1,\ldots M, \qquad (5)$$

where the first M_g values of $y_k(\mathbf{r}_i)$ are known: $M = 40$ and $M_g = 16$.

Let us consider the populations of particles settled on the surface in the form of free particles and particle aggregates (F- and A-populations, respectively). Let us introduce the following assumptions.

(i) The A-population was completely formed within the release source Ω at the stage of convective uplift of the gas suspension or in the eruptive cloud, so that no exchange takes place between F- and A-populations during transport in the atmosphere.

(ii) Ejected mass distributions on the masses of individual particles and on the rates of particles' precipitation in the source do not depend on altitude (conditions of uniform fraction and component composition of a suspension of gas and ash).

(iii) For an individual particle, v_t is determined by the d, ρ, and F parameters in the F-population and by the diameter $d_{(A)}$ and density $\rho_{(A)}$ of ash aggregate in the A-population (this aggregate includes an individual particle and its shape is considered to be spherical).

(iv) Variations in v_t within any given grain size class can be taken into account by considering one or several "representative" F- and A-subpopulations, each of which has the abovementioned parameters varying within quite narrow ranges.

The assumptions (i)–(iv) are validated a posteriori from model calculation results; however, they are also reasonable from the physical viewpoint. Indeed, mean vertical (ordered and turbulent) transport rates in the eruptive column exceed those of gravity precipitation in the entire considered range of grain sizes of free par-

ticles (see Figs. 6b and 7) and ash aggregates multiple times, and thus the gravity differentiation of finely dispersed ash material in the zone of its convective transport is run not very intensively.

In general, constraint (ii) is stronger for A-population, if we take the broad variation range of thermodynamic parameters controlling the formation of ash aggregates both within the eruptive column and in the surrounding atmosphere. However, it should be taken into account that ash aggregates in reality can form in a broad range of altitudes, and more or less reliable numerical models of this process are unavailable at the moment. The thermodynamic parameters of the eruptive column, calculated by the PlumeRise model, show, in particular, that for the eruption of December 24, 2006, water vapor condensation in the eruptive column may have started at the altitude of about 6.6 km, at the altitudes of 7.3–8.7 km the water may have been in a liquid phase, and, rising higher, water may have turned to ice. The presence of igneous water in the background of the relatively high background air humidity (>90% at the altitudes of less than 2 km and ~70% in the upper troposphere) may have created extremely favorable conditions for ash aggregates to form in almost the entire range of ash release, excluding the lowermost part of the eruptive column. The evidence in favor of this suggestion is from direct observations in the ashfall zone of the considered eruption, at Klyuchi settlement. The snowfall observed during the ashfall may have been caused by or been directly related to the formation of ash aggregates by gravity coagulation in the interaction of ash particles with hydrometeors [35].

Following [18], in each grain size class, we present the initial $F \cup A$ population as the sum of F_p- ($p = 1,...P_1$) and A_q-subpopulations ($q = 1,...P_2$; in the given example, $P_1 = P_2 = 5$). We assume $F = 0.1(2p - 1)$ and $\rho = 2.4$ g/cm^3 for F_p particles; $d_{(A),\,\min} = 250$ μm, $d_{(A),\,\max} = 250$ μm, and $\rho_{(A)q} = 0.5q$ g/cm^3 for A_q. Let us express total masses of $F_{1,...P_1}$ and $A_{1,...P_2}$ subpopulations (indices $s = 1,...P_1$ and $s = P_1 + 1,... S$, respectively) in terms of $\alpha_s^{(k)}$, $s = 1...S(= P_1 + P_2)$ in such a way that

$$(\mathrm{TRM})_k(\mathrm{F} \cup \mathrm{A}) = \alpha_1^{(k)} + \alpha_2^{(k)} .... + \alpha_S^{(k)}, \quad (6)$$

$$(\mathrm{TRM})_{<500j} = \beta_j \sum_{k=k_1}^{k_2} (\mathrm{TRM})_k, \quad (7)$$

where β_j is the mass distribution (in fractions of 1) on altitude. Then let us assume $\alpha_s^{(k)}$ to be uniformly distributed over the logarithms of masses of individual particles $m_{(F)}$ and as aggregates $m_{(A)}$ within F- and A-subpopulations, respectively. Then the joint density of $(\mathrm{TRM})_k$ distribution on masses of individual particles will have the following form:

$$t^{(k)}(m) = \sum_{s=1}^{S} t_s^{(k)}(m) = c_1 \sum_{s=1}^{S} \alpha_s^{(k)} m^{-1}, \quad (8)$$

where $m \equiv m_{(F)} (i \le P_1)$, $m \equiv m_{(A)} (i = P_1 + 1,...S)$, $c_1 = (3 \ln 2)^{-1}$ is the normalization factor.

In terms of the Lagrangian approach to describing atmospheric transport [36], the general solution of the direct problem that links the field of precipitated mass to the point ($\mathbf{r}$) and the TRM distribution in the source, with (i)–(iv) and (6)–(8) taken into account, can be written as follows:

$$y^{(k)}(\mathbf{r}_i) = \sum_{j=1}^{N} \beta_j R_j^{(k)}(\mathbf{r}_i; \boldsymbol{\alpha}^{(k)}), \quad (9)$$

$$R_j^{(k)}(\mathbf{r}; \boldsymbol{\alpha}^{(k)}) = \sum_{s=1}^{S} \alpha_s^{(k)} Q_{s,j}^{(k)}(\mathbf{r}), \quad (10)$$

where $\boldsymbol{\alpha}^{(k)} = (\alpha_1^{(k)},...\alpha_S^{(k)})$,

$$Q_{s,j}^{(k)}(\mathbf{r}) = c_1 \int\limits_{\mathbf{r}' \in \varpi_j} d^3\mathbf{r}' \int\limits_{m \in M_s^{(k)}} G_s(\mathbf{r}' \to \mathbf{r} | v_t) \partial \log m,$$

where $M_s^{(k)}$ is the range of variation for masses of k particles from the s-subpopulation; G is the probability of transport for a particle with precipitation rate v_t, from any point $\mathbf{r}' \in \varpi_j$ to the point $\mathbf{r}$ on the Earth surface; and interval $(\cdot; \boldsymbol{\alpha}^{(k)})$ indicates the parametric dependence of functionals $R_j^{(k)}$ on $\boldsymbol{\alpha}^{(k)}$.

Due to (6) and (7), the problem of defining the source parameters is therefore reduced to defining the coefficients $\boldsymbol{\beta} = (\beta_1,...\beta_N)$, $\boldsymbol{\alpha}^{(k)}$, and $k = k_1,...k_2$ based on the measurements of $\mathbf{y}_{\mathrm{obs}}$ and $\mathbf{y}_{\mathrm{obs}}^{(k)}$, and the values of Green functions G_s from the model. With the low dimension of the data space, we will search for the first approximation of the exact solution (9)–(10) on the basis of the following two-step algorithm.

At step 1, we calculate coefficients $\alpha_s^{(k)}$ in terms of the approximation of spatially uniform source [18]. Substituting (10) in (9) at $\beta_j \equiv N^{-1}$ leads to the problems of the relatively sought $\alpha_s^{(k)}$:

$$\hat{\boldsymbol{\alpha}}^{(k)} = \arg\min_{\boldsymbol{\alpha}^{(k)}} \left\| \mathbf{y}_{\mathrm{obs}}^{(k)} - \mathbf{C}^{(k)} \boldsymbol{\alpha}^{(k)} \right\|, \quad k = k_1,...k_2, \quad (11)$$

where $\mathbf{C}^{(k)}$ is the $(M_g \times S)$-matrix with elements $(\mathbf{C}^{(k)})_{i,s} = Q_{s,1}^{(k)}(\mathbf{r}_i) + ...Q_{s,N}^{(k)}(\mathbf{r}_i)$, $\|\mathbf{a}\| (\equiv \mathbf{a}^T \cdot \mathbf{a})$ denotes the Euclidean norm of vector ($\mathbf{a}^T$ is the conjugation symbol). The solution of (11) was based on the best subset of predictors among all $2^S - 1$ possible combinations [37, Ch. 6]. One of the benefits of this approach (in terms of the problem under consideration), compared to other

methods of regularization, is the clear physical interpretation of the obtained result. Indeed, such an approach allows us to choose the most representative particle subpopulations forming the resultant spectrum of precipitation rates in *F*- and *A*-populations [18].

Substitution of the coefficients $\hat{\boldsymbol{\alpha}}^{(k)}$ found at the first step in (9), with the subsequent summation on k, leads us to a system consisting of M equations relative to the sought β_j (step 2). The poor conditioning of this system is caused by correlation between the fields of precipitated mass from sources at different altitudes; the statistical availability of the obtained estimates also considerably varies between particular ranges of the ash release height. With these peculiarities in mind, the solution of the obtained system was built in terms of the optimization problem [38, 39]:

$$\boldsymbol{\beta}_\tau = \arg\min_{\boldsymbol{\beta}} \{\|\mathbf{y} - \mathbf{B}\cdot\boldsymbol{\beta}\| + \tau\cdot\|\mathbf{L}_2\cdot\boldsymbol{\beta}\|\}, \qquad (12)$$

where $\mathbf{B}$ is a $(M \times N)$-matrix with elements $(\mathbf{B})_{i,j} = R_j^{(k_1)}(\mathbf{r}_i;\hat{\boldsymbol{\alpha}}^{(k_1)}) + \ldots R_j^{(k_2)}(\mathbf{r}_i;\hat{\boldsymbol{\alpha}}^{(k_2)})$, τ is the regularization parameter; $\mathbf{L}_2$ is the matrix operator of second derivative on z. Application of the stabilizing functional $\mathbf{L}_2\cdot\boldsymbol{\beta}$ allows us to reconstruct mass distribution on altitudes with the maximal detail, which is possible in terms of the chosen regression model and the model source, with the suppressed contribution of the solution components with the greatest variation (corresponding to small singular numbers $\mathbf{B}$) at the level of measurement data noise [38–40]. The solution of (12) was based on the numerical algorithm [41, Ch. 25].

The choice of optimal $\hat{\boldsymbol{\alpha}}^{(k)}$ at the step 1 and $\tau = \tau*$ at the step 2 was made on the basis of PRESS statistics (the predicted mean square deviation, $\mathrm{MSD_{PR}}$, between the calculated and the measured precipitated masses [37, Ch. 6]). In solving (13), two methods were used. These methods differ in the way that measurement data were taken into account: in method 1, $\boldsymbol{\beta}$ was calculated with the use of all measurements, while in method 2, only the 16 first samples, whose grain size composition had been taken into consideration at the step 1, were considered; PRESS statistics for both methods were calculated for the entire set of $I = 1,\ldots M$. We also used two auxiliary statistics as a general measure of agreement: MSD for points with zero measured bulk masses ($\mathrm{MSD_0}$) and sign function γ, which was defined over the entire set of measurements (49 points) and was the quantitative expression of the general shift between the calculated and the measured precipitated masses:

$$\gamma = |n(+) - n(-)|/(n(+) + n(-)), \qquad (13)$$

where $n(+)$ and $n(-)$ are the numbers of the points at which the calculated masses were higher and lower than the measured, respectively [15].

The mentioned statistics, as functions of τ, are given in Fig. 6. We can see that the solution of (12) by both methods stabilized in a broad range of $\tau = 0.01$–$0.1\lambda_1$ (λ_1 is the main singular number of matrix $\mathbf{BL}_2^{-1}$); the resultant estimates of the total released ash mass and its distribution in altitude (Fig. 10) generally agree with each other. The presence of nonzero $\mathrm{MSD_0}$ in the entire range of τ indicates a small systematic component of reconstruction error for the precipitated mass field: it manifests, in particular, in some overestimation of the ashfall area (see Fig. 12 below). However, the results of method 1 ($\sim 3.6 \times 10^9$ kg) seem to be generally underestimated in comparison to the probable range of real released ash mass estimated by different methods [18] at $(3.8$–$5.1) \times 10^9$ kg, despite the fact that, in such an approach, the amount of data used for calculation of $\boldsymbol{\beta}$ at step 2 appears to be greater by a factor of 2.5. We can conclude that, in the considered case, the subdivision of the initial data set into the "estimation" and "validation" subsets enables us to obtain more realistic estimates owing to the more objective criteria of fit between the model and observations.

3.6. Model Calculations

Meteorological fields were calculated on three finite-difference grids: an outer one, G1 (50×50 nodes, horizontal size of a cell is $\Delta x = 60$ km); an intermediate one, G2 (70×70 nodes, horizontal size of a cell is $\Delta x = 15$ km); and an inner one, G3 (107×107 nodes, horizontal size of a cell is $\Delta x = 3$ km). All grids are centered on the volcano (Fig. 9). For all grids, a similar vertical geometry was used: 40 calculation levels with an upper boundary at an altitude of 22.7 km and a step gently increasing from 200 m at <1 km to 700 m above the tropopause. In order to set the initial and boundary conditions in the model, we used $1^\circ \times 1^\circ$ meteorological fields from NCEP FNL analysis (ds083.2 database) for 00:00 and 23:00 GMT.

The calculations on RAMS were performed for the period from December 23, 2006, 00:00 GMT to December 24, 2006, 15:00 GMT, for sequential intervals of 10 min. The detailed description of the structure of the model meteorological fields in the vicinity of volcano and the influence of meteorological fields on the precipitation conditions of ash particles is given in [18]. Preliminary numerical experiments have shown that particles from the $\mathrm{F_{<63\,\mu m}}$ fraction precipitated nearly completely in the form of aggregates, while those of the more coarse-grained fractions ($\mathrm{F_2}$ and $\mathrm{F_3}$) precipitated as individual particles. The fraction $\mathrm{F_4}$ contained particles from both populations. In the final calculations, we simulated the transport of $F_{1,\ldots5}$-subpopulations in the fractions $\mathrm{F_2}$, $\mathrm{F_3}$, and $\mathrm{F_4}$ and that of $A_{1,\ldots5}$-subpopulations in the fractions $\mathrm{F_3}$ and $\mathrm{F_4}$. Thus, for each of 12 model sources ϖ_j we considered 25 subpopulations, each of which included 10^4

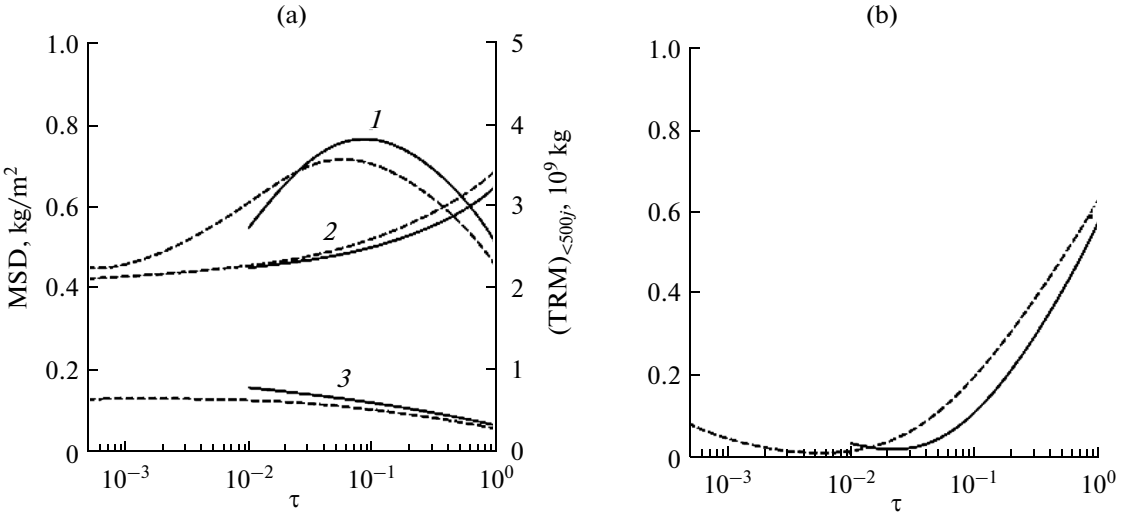

Fig. 8. Dependence of $(TRM)_{<500,j}$ (*1*), MSD_{PR} (*2*), MSD_0 (3a), and γ (3b) on τ when solving (12) by methods 1 (dashed line) and 2 (solid line) (see section 3.5).

HYPACT model particles (in total, 25 × 12 × × 10^4 to 3 × 10^6 model particles).

4. RESULTS

The distribution of the released ash mass on altitudes $(TRM)_{<500,j}$ (as reconstructed by method 2 at $\tau^* = 0.03$), the comparison between calculated$y_{clc}(\mathbf{r}_i)$ and measured $y_{obs}(\mathbf{r}_i)$ masses at the sampling points, and the model field of precipitated ash mass $y_{clc}(\mathbf{r})$ are presented in Figs. 10–12, respectively. Let us give the calculated mass-release parameters (in parentheses, standard deviations of estimates):

Altitudes above sea level, km	2–6	6–14
Mass release, Mt:	0.78 (±0.15)	3.36 (±0.30)
$(TRM)_{<500} = 4.13\ (\pm 0.40) 10^9$ kg		

The summarized grain size of ash release $(TRM)_k/(TRM)_{<500}$ 100%:

Fractions, mm	<63	63–125	125–250	250–500
$(TRM)_k$, wt %:	57.6	14.9	19.2	8.3

The main contribution to the error of $(TRM)_{<500}$ vertical profile reconstruction is made by errors related to the definition of total mass in particular subpopulations ($\alpha_i^{(k)}$ coefficients) at step 1. The regular decrease in relative errors of $(TRM)_{<500,j}$ value reconstruction with altitude (Fig. 10) is caused by the greater statistical availability of resultant estimates for higher altitudes (a greater amount of sampling points where particles from the *j*-th source were found) in the eruptive cloud, from where most particles precipitate.

The calculated value of $(TRM)_{<500}$ agrees, within error, with the total precipitated mass of ash particles (3.8× 10^9 kg) estimated by the isopach method [9]. The relatively large amount of sampling points for the discussed explosive event allows us to consider the value of 3.8 × 10^9 kg as a quite reliable one, despite the absence of objective quantitative criteria to estimate errors appearing in the application of this method.

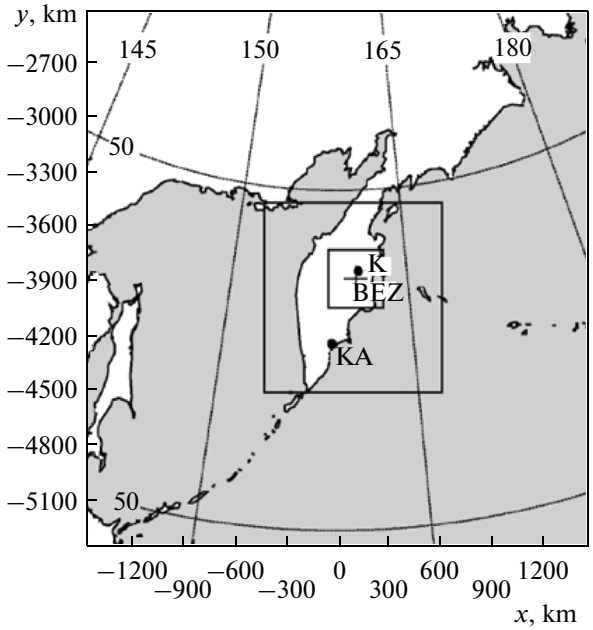

Fig. 9. Calculated G1, G2, and G3 zones of RAMS model. Aerological probing stations: KL, Klyuchi: KA, Kamchatskaya. BEZ, Bezymyanny volcano. *x* and *y* are the horizontal coordinates on G1 field in polar stereographic projection.

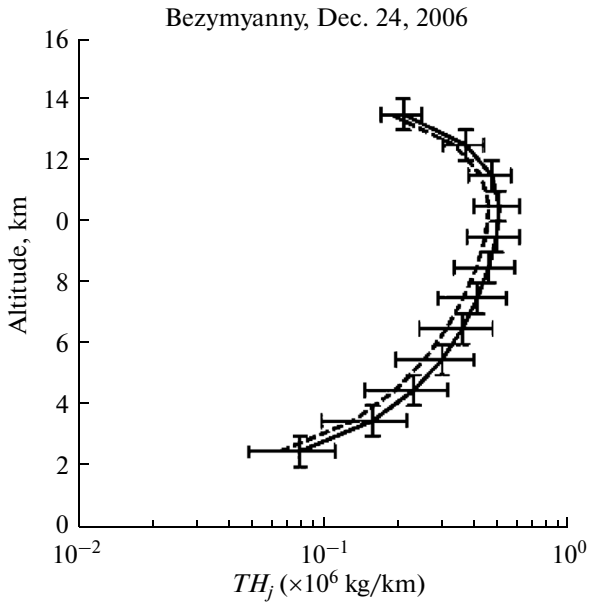

Fig. 10. Total released ash masses in particular altitude intervals as reconstructed by methods 1 (dashed line) and 2 (solid line) for the eruption of Bezymyanny volcano on December 24, 2006. Vertical lines denote ash release intervals (a km step) fro the model sources; horizontal ones, standard deviations for the reconstructed values of $(TRM)_{<500,j}$.

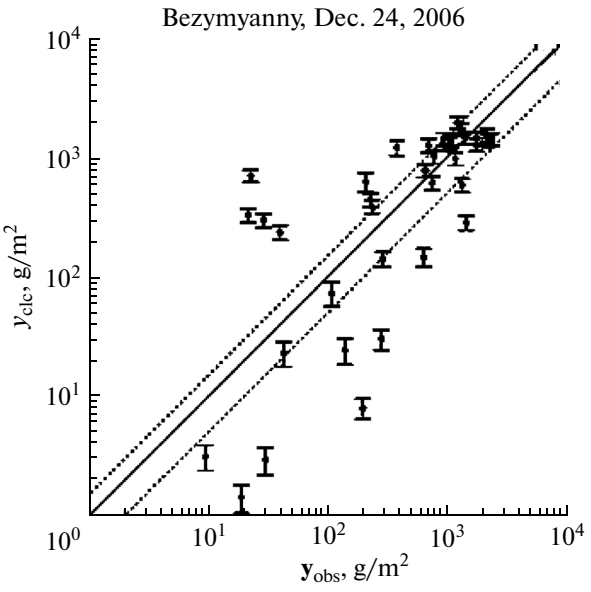

Fig. 11. The calculated $\mathbf{y}_{clc}$ and measured $\mathbf{y}_{obs}$ masses of precipitated ash in the ashfall zone during the eruption of Bezymyanny volcano on December 23–24, 2006. Dashed lines confine the double MSD variation interval of $\mathbf{y}_{clc}$ for the reconstructed value of the total released mass.

However, in our opinion, the observed difference of 0.33 Mt is of a systematic character and is related to the known feature of the isopach method (underestimation of the real precipitated ash mass in the absence of ash samples in the near zone (<20 km) of volcano, where ash material may have precipitated from PFs and from the lower part of eruptive cloud). The value obtained by the isopach method can be therefore considered as an independent lower estimate of the total precipitated ash when validating the regression model.

The reconstructed distribution of the released ash mass (Fig. 10) agrees with a priori ideas about the predominant removal of ash material to the upper part of eruptive column at the sub-Plinian phase of eruption. The profiles calculated by methods 1 and 2 show a good agreement between each other at small, although systematic, underestimation of released ash mass by method 1 in the entire range of altitudes. Nearly half of the released ash mass (2.1×10^9 kg) falls at altitudes of 9–14 km, corresponding to the upper part of eruptive column, near and above the neutral buoyancy zone (~9.5 km high), where the freely ascending convective flow transforms to the gravity density flow (eruptive cloud) and then to the lee side plume. It should be noted, however, that a noticeable part of the released ash mass (0.78×10^9 kg) falls at altitudes <6 km, which are considerably below the neutral buoyancy zone; this can be explained, in part, by the involvement of a certain part of ash material from the marginal parts of the eruptive column into the cross flow. Another possible ash source at these altitudes could be ash clouds of PFs (see section 2.1). It is known that the grain-size composition of ashes from PF clouds are characterized by a higher content of fine fractions, compared to ashes precipitating at the same distances from an eruptive cloud [42–44]. Based on measurements, the highest content of particles of <125 μm in size was in samples collected at a distance of 40 km WNW (93.3 wt %, 116 g) and 23 km W of the volcano (88 wt %, 148 g). For these samples, the contribution of transport from model sources at altitudes of <6 km (Fig. 3, points in the zones marked as PFs) absolutely dominated in comparison to samples collected at the same distances, but with a predominant contribution (66.0–80.8 wt %) of ash precipitated from higher altitudes. Based on observations at Bezymyanny volcano [42], the following approximate ratio was obtained:

$$H_{PF} \cong 8\text{–}10h_F,$$

where H_{PF} is the height of PF clouds from the Earth's surface and h_F is the width of the PF front. For the considered event, $h_F \approx 425$ m, hence we obtain $H_{PF} \approx 4$ km (or 5.5–6 km on absolute height), and this value agrees with the model prediction.

The comparison between the calculated and measured ash masses in the sampling points is shown in Fig. 11 (determination factor $R^2 = 0.8$, MSD = 480 g/m^2, $MSD_0 = 138$ g/m^2). Depending on the value of the measured ash mass $y_{obs,i}$, points in the plot

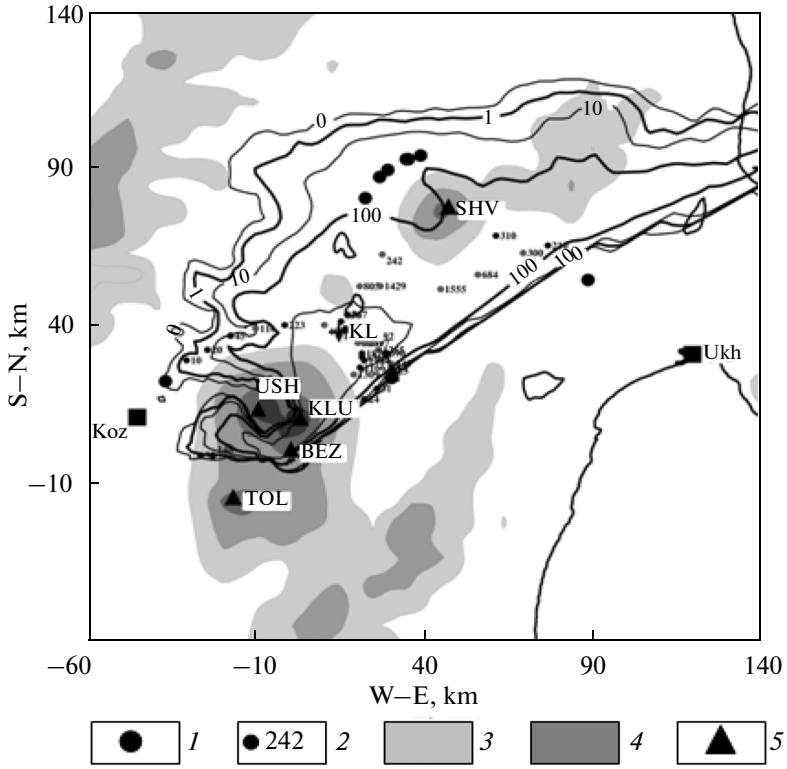

Fig. 12. The calculated field of precipitated volcanic ash mass (g/m^2) at the optimal model parameters of ash release. (*1*) and (*2*) points with measured ash mass of <1 and >1 g/m^2, respectively; (*3*) and (*4*) zones with model altitudes of >500 and >1000 m, respectively; (*5*) volcanoes (SHV, Shiveluch; KLU, Klyuchevskoy; BEZ, Bezymyanny; USH, Ushakovsky massif; TOL, Plosky Tolbachik). Settlements and towns: KL, Klyuchi; Koz, Kozyrevsk; Ukm, Ust-Kamchatsk.

are subdivided into two groups. As was mentioned above, the field of ash precipitations is generally characterized by the presence of a clearly expressed upwind-side boundary, in whose vicinity the spatial gradients of precipitated mass are high, and a diffuse lee-side boundary (Figs. 4 and 12), whose position is largely controlled by topographic inhomogeneities of a sub-mesh scale. The presence of both features leads to the highest errors in the calculation of precipitated ash mass near the ashfall boundary, where the measured bulk masses are small. For 28 points with $y_{obs,\,i} >$ 200 g/m^2, which correspond to the measurements within the main ash-precipitation zone, there is a satisfactorily good fit between the observed mass and model calculations, without any considerable shift of the model estimates (MSD = 412 g/m^2, $n(+) = 16$, $n(-) = 12$). Remarkably, the most sampling points (18 of 26) falls within the uncertainty interval correspond-

Data on ash sampling for the eruption of Bezymyanny volcano on December 24, 2006

Measurements	M	ΔL, km	d_{max}, μm	m, kg/m^2	m_{63} (wt %)
Total mass	40	23–105	<1000	0.001–2.56	–
Points with nonzero mass	9	38–104	–	0.000	–
Screen analysis	16	23–93	<500	0.116–2.56	55–84

M is the number of sampling points; ΔL is the distance from the volcano; d_{max} is the maximal size of particles; m is the mass of ash particles in samples; m[63] is the content of fine particles (<63 μm in size) in samples.

ing to the double standard deviation for estimating the total released ash mass.

CONCLUSIONS

The approach described in the present work allows researchers to correctly take into account the main factors responsible for the transport and precipitation of ash material on a mesoscale and to obtain the agreed numerical estimates of the total released ash mass and the ashfall distribution at altitudes. The proposed method should be considered as a supplementary one to the existing methods for TRM estimation, including those based on the measurements of the heights of eruptive clouds and plumes [34, 45, 46], on satellite measurement data [47], and on the estimates of the energy parameters of eruption from the recorded seismic [48] and acoustic [49] signals. It seems that at the present state of the art, when analyzing concrete explosive events, the most reliable estimates of the ash release parameters can be obtained by using an "ensemble" approach, with all possible data involved. Nevertheless, an obvious advantage of the proposed approach is the direct application of mass parameters characterizing the concrete explosive event (mass of ash precipitated in sampling points and results of grain size analysis). Thus one of the main sources of error is eliminated; this source of error is typical for all remote methods and is related to the necessity of recalculation of the measured energy parameters (in the case of satellite measurements, integrated optical parameters) into parameters of released ash mass. These parameters can be used, in particular, for specifying ashfall scenarios of the currently active volcanoes in Kamchatka in terms of models of real-time ash cloud forecast used by the international Volcanic Ash Advisory Centres (VAAC) [46, 50]. The abilities of the developed numerical algorithm will be studied in more detail by using field-observation data for other explosive eruptions.

ACKNOWLEDGMENTS

The work was supported by the Far East Branch of the Russian Academy of Sciences (grant no. 14-III-V-08-015) and by the Russian Foundation for Basic Research (project no. 14-35-50453).

REFERENCES

1. A. Robock, "Volcanic eruptions and climate," Rev. Geophys. **38** (2), 191–219 (2000).
2. S. Self, "The effects and consequences of very large explosive volcanic eruptions," Philos. Trans. R. Soc. Am. **364**, 2073–2097 (2006).
3. A. V. Eliseev and I. I. Mokhov, "Influence of volcanic activity on climate change in the past several centuries: Assessments with a climate model of intermediate complexity," Izv., Atmos. Ocean. Phys. **44** (6), 671–683 (2008).
4. Yu. B. Slezin, *Mechanism of Volcanic Eruptions (Stationary Model)* (Nauchnyi mir, Moscow, 1998) [in Russian].
5. M. Alidibirov and D. B. Dingwell, "Magma fragmentation by rapid decompression," Nature **380**, 146–148 (1996).
6. A. A. Barmin and O. E. Mel'nik, "Hydrodynamics of volcanic eruptions," Usp. Mekh. **1** (1), 32–60 (2002).
7. I. I. Gushchenko, *Ashes from North Kamchatka and Conditions of their Formation* (Nauka, Moscow, 1965) [in Russian].
8. D. M. Pyle, "The thickness, volume and grainsize of tephra fall deposits," Bull. Volcanol. **51** (1), 1–15 (1989).
9. J. Fierstein and M. Nathenson, "Another look at the calculation of fallout tephra volumes," Bull. Volcanol. **54**, 156–167 (1992).
10. A. W. Hurst, *ASH-FALL—A computer Program for Estimating Volcanic Ash Fallout. Report and Users Guide* (Institute of Geological and Nuclear Sciences, Wellington, 1994).
11. A. W. Hurst and R. Turner, "Performance of the program ASH-FALL for forecasting ashfall during the 1995 and 1996 eruptions of Ruapehu volcano, New Zealand," J. Geol. Geophys. **42** (4), 615–622 (1999).
12. G. Macedonio, A. Costa, and A. Longo, "A computer model for volcanic ash fallout and assessment of subsequent hazard," Comput. Geosci. **31** (7), 837–845 (2005).
13. C. Bonadonna, G. Macedonio, and R. S. J. Sparks, "Numerical modelling of tephra fallout associated with dome collapses and Vulcanian explosions: Application to hazard assessment on Montserrat, in *The Eruption of Soufrière Hills Volcano, Montserrat, from 1995 to 1999*, Ed. by T. H. Druitt and B. P. Kokelaar (Geological Society of London, London, 2002), pp. 517–537.
14. R. Bonasia, G. Macedonio, A. Costa, et al., "Numerical inversion and analysis of tephra fallout deposits from the 472 AD sub-Plinian eruption at Vesuvius (Italy) through a new best-fit procedure," J. Volcanol. Geotherm. Res. **189**, 238–246 (2009).
15. L. J. Connor and C. B. Connor, *Inversion is the key to dispersion*: Understanding eruption dynamics by inverting tephra fallout, in *Statistics in Volcanology. Special Publications of IAVCEI*, Ed. by H. M. Mader, S. G. Cole, C. B. Connor, and L. J. Connor (Geological Society of London, London, 2006), pp. 231–242.
16. A. C. M. Volentik, C. Bonadonna, C. B. Connor, et al., "Modeling tephra dispersal in absence of wind: Insights from the climactic phase of the 2450 BP Plinian eruption of Pululagua volcano (Ecuador)," J. Volcanol. Geotherm. Res. **193** (1–2), 117–136 (2010).
17. N. A. Malik, "The December 24, 2006 eruption of Bezymyannyi volcano, Kamchatka," J. Volcanol. Seismol. **5** (4), 268–277 (2011).
18. K. B. Moiseenko and N. A. Malik, "Estimates of total ash content from 2006 and 2009 explosion events at Bezymianny volcano with use of a regional atmospheric modeling system," J. Volcanol. Geotherm. Res. **270**, 53–75 (2014).

19. K. B. Moiseenko and N. A. Malik, "Estimation of total discharges of volcanic ash using atmospheric-transport models," J. Volcanol. Seismol. **9** (1), 30–47 (2015).

20. A. I. Malyshev, *The Life of Volcano* (UrO RAN, Yekaterinburg, 2000) [in Russian].

21. O. A. Girina, "Chronology of Bezymianny volcano activity, 1956–2010," J. Volcanol. Geotherm. Res. **263**, 22–41 (2013).

22. A. J. Carter, O. A. Girina, M. S. Ramsey, and Yu. V. Demyanchuk, "ASTER and field observations of the 24 December 2006 eruption of Bezymianny volcano, Russia," Remote Sens. Environ. **112**, 2569–2577 (2008).

23. C. J. Tremback, W. A. Lyons, W. P. Thorson, and R. L. Walko, "An emergency response and local weather forecasting software system", in *Eighth Joint Conf. on Applications of Air Pollution Meteorology with A&WMA* (American Meteorological Society, Nashville, Tennessee, 1994), pp. 219–223.

24. R. A. Pielke, W. R. Cotton, C. J. Tremback, et al., "A comprehensive meteorological modeling system—RAMS," Meteorol. Atmos. Phys. **49**, 69–91 (1992).

25. R. L. Walko and C. J. Tremback, *HYPACT; the Hybrid Particle and Concentration Transport Model. User's Guide* (Mission Research Corporation, Ft Collins, 1995).

26. G. L. Mellor and T. Yamada, "Development of a turbulence closure model for geophysical fluid problems," Rev. Geophys. Space Phys. **20**, 851–875 (1982).

27. H. M. Helfand and J. C. Labraga, "Design of a nonsingular level 2.5 second-order closure model for the prediction of atmospheric turbulence," J. Atmos. Sci. **45**, 113–132 (1988).

28. R. Turner and T. Hurst, "Factors influencing volcanic ash dispersal from the 1995 and 1996 eruptions of Mount Ruapehu, New Zealand," J. Appl. Meteorol. **40**, 56–69 (2001).

29. L. Wilson and T. Huang, "The influence of shape on the atmospheric settling velocity of volcanic ash particles," Earth Planet. Sci. Lett. **44**, 311–324 (1979).

30. G. T. Csanady, "Turbulent diffusion of heavy particles in the atmosphere," J. Atmos. Sci. **20** (3), 201–208 (1963).

31. L.-P. Wang and D. E. Stock, "Dispersion of heavy particles in turbulent motion," J. Atmos. Sci. **50** (13), 1897–1913 (1993).

32. P. J. Walklate, "A Markov-chain particle dispersion model based on airflow data: Extension to large water droplets," Boundary-Layer Meteorol. **37**, 313–318 (1986).

33. P. J. Walklate, "A random-walk model for dispersion of heavy particles in turbulent air flow," Boundary-Layer Meteorol. **39**, 175–190 (1987).

34. M. J. Woodhouse, A. J. Hogg, J. C. Phillips, and R. S. J. Sparks, "Interaction between volcanic plumes and wind during the 2010 Eyjafjallajökull Eruption, Iceland," J. Geophys. Res. **118** (1B), 92–109 (2013).

35. R. J. Brown, C. Bonadonna, and A. J. Durant, "A review of volcanic ash aggregation," Phys. Chem. Earth **45–46**, 65–78 (2012).

36. A. S. Monin and A. M. Yaglom, *Statistical Hydromechanics*, Vol. 1 (Nauka, Moscow, 1965) [in Russian].

37. N. R. Draper and H. Smith, *Applied Regression Analysis* (Wiley, New York, 1981).

38. P. C. Hansen, "Regularization, GSVD and truncated GSVD," BIT **29**, 491–504 (1989).

39. A. Hocker and V. Kartvelishvili, "SVD approach to data unfolding," Nucl. Instrum. Methods A **372**, 469–481 (1996).

40. A. N. Tikhonov and V. Ya. Arsenin, *Methods for Solving Ill-Posed Problems* (Nauka, Moscow, 1979) [In Russian].

41. C. L. Lawson and R. J. Hanson, *Solving Least Squares Problems* (Prentice-Hall, Englewood Cliffs, 1974).

42. O. A. Girina, *Pyroclastic Formations of Current Eruptions of Andesite Volcanoes in Kamchatka and Their Engineering and Geological Features* (Dal'nauka, Vladivostok, 1998) [in Russian].

43. O. A. Girina, "Convective gravitational differentiation of pyroclastics of andesite volcanoes," Litosfera, No. 3, 135–144 (2010).

44. J. R. Evans, J. E. Huntoon, W. I. Rose, et al., "Particle sizes of andesitic ash fallout from vertical eruptions and co-pyroclastic flow clouds, Volcan De Colima, Mexico," Geology **37** (10), 935–938 (2009).

45. S. A. Fedotov, "Estimate for heat and pyroclastic removal by volcanic eruptions and fumaroles on the basis of height of their jets and clouds," Vulkanol. Seismol., No. 4, 3–28 (1982).

46. L. G. Mastin, M. Guffanti, R. Servranckx, et al., "A multidisciplinary effort to assign realistic source parameters to models of volcanic ash–cloud transport and dispersion during eruptions," J. Volcanol. Geotherm. Res. **186** (1–2), 10–21 (2009).

47. A. V. Rybin, M. V. Chibisova, P. Webley, et al., "Satellite and ground observations of the June 2009 eruption of Sarychev Peak volcano, Matua Island, Central Kuriles," Bull. Volcanol. **73** (9), 1377–1392 (2011).

48. E. R. Makhmudov, P. P. Firstov, and Yu. T. Kozhevnikova, "Seismic effects accompanying the eruptions of Bezymianny volcano (Kamchatka), in *Natural Disasters: Research, Monitoring, Forecast. Proceedings of the 5th Sakhalin Young Scientific School, Yuzhno-Sakhalinsk, June 8–11, 2010* (IMGG FEB RAS, Yuzhno-Sakhalinsk, 2011), pp. 178–185.

49. P. P. Firstov, "Specific features of acoustic and seismic waves accompanying the eruption of Bezimmyannii in 1983–1985," Vulkanol. Seismol., No. 2, 81–97 (1988).

50. O. A. Girina and E. I. Gordeev, "The project KVERT—decline in volcanic hazard for aviation during explosive eruptions of volcanoes in Kamchatka and North Kuril," Vestn. DVO RAN, No. 2 132 (2007).

Translated by N. Astafiev